Higher Order Mode Probes in Spherical Near-Field Measurements

Allen C. Newell, Stuart F Gregson
Nearfield Systrems Inc, 19730 Magellan Drive, Torrance, CA 90502, USA
allen_newell@qwestoffice.net, sgregson@nearfield.com

Abstract— **A previous study** (1) **by the authors reported on a computer simulation using Open Ended Waveguide probe data and actual test antenna data to quantify the effect of using higher order probes with the spherical processing that assumes the probe has only μ = ±1 modes. That study was based on the observation that since the higher order probe's azimuthal modes are directly related to the probe's properties for rotation about its axis, the near-field data that should be most sensitive to these modes is a near-field polarization measurement. Such a measurement would be taken with the probe at a fixed (θ,φ,z) position and the probe is then rotated about its axis by the angle χ over 360 degrees. The amplitude and phase received by the probe would be measured as a function of the χ rotation angle. A direct measurement using different probes would be desirable, but since the effect of the higher order modes is very small, other measurement errors would likely obscure the desired information. A computer simulation rather than a measurement was therefore used where the plane-wave transmission equation was used to calculate the received signal for an AUT/probe combination where the probe is at any specified position in the near-field. The plane wave spectra for both the AUT and the probe were derived from measured planar data for the AUT and spherical near-field data for the probe. The plane wave spectrum for the AUT was the same for all calculations with the main beam along the Z-axis and the AUT at the origin. The receiving spectrum for the probe at each (θ,φ,χ) orientation was determined from the far-field pattern of the probe after it had been rotated by χ . The far-field pattern of the probe as derived from spherical near-field measurements can be filtered to include or exclude the higher order spherical modes, and the near-field polarization data can therefore be calculated to show the sensitivity to these higher order modes. This approach focuses on the effect of the higher order spherical modes and completely excludes the effect of measurement errors.**

The study indicated that the effect of the higher order probes on the measured near-field data was on the order of 50 dB below the peak of the near-field data and would likely be below the effect of other errors such as scattering, alignment, and total system random errors. Two test antennas were used in the previous study, and a limited number of probe positions were used in the simulation. The results described in this paper extends the initial study to include additional simulation results that are more representative of a spherical near-field measurement. For the current simulations, the AUT pattern is first rotated about the Y-axis to simulate off-axis θ angles on the measurement sphere and the probe z position is varied to simulate different measurement radii.

Index Terms—spherical, near-field, measurements, OEWG probes, uncertainty analysis, spherical modes, high order probes.

I. INTRODUCTION

The spherical near-field theory is based on the transmission equation derived by Jensen (2) – (3) and further developed by Wacker (4) where the antenna under test and the probe are described by spherical mode coefficients that are the coefficients of basis functions that are solutions of Maxwell's equations for a spherical coordinate system. In principle, the transmission equation is valid for any arbitrary test antenna and probe combination at any separation distance between the spherical coordinate system origin and the probe that is outside of the minimum sphere that will completely enclose the antenna under test. The transmission equation is,

$$W^a(\chi,\phi,\theta)=\sum_m\sum_n\sum_\mu\left(\sum_{s=1}^{2}P^{s\mu na}\,Q^{smn}\right)e^{im\phi}\,d^{(n)}_{m\mu}(\theta)\,e^{i\mu\chi}. \quad (1)$$

Where W^a represents the amplitude and phase data measured by the probe at the radius a and the position defined by the spherical coordinates θ *and* ϕ. χ is the rotation angle of the probe about its z-axis. The P's are the spherical mode coefficients for the probe and the Q's are the corresponding spherical mode coefficients for the antenna under test. Mathematical orthogonality is used to solve the transmission equation in order to obtain the coupling product which is the product within the brackets of equation 1. The result is shown in equation 2.

$$I^{m'\mu'n'a}=\frac{1}{8\pi^2}\int_0^{2\pi}\int_0^{2\pi}\int_0^{2\pi}W^a(\chi,\theta,\phi)\left(e^{-im'\phi}\,d^{(n')}_{m'\mu'}(\theta)\,e^{i\mu'\chi}\right)\times\sin\theta\,d\theta\,d\phi\,d\chi \quad (2)$$

Where,

$$I^{m'\mu'n'a}=P^{1\mu'n'a}\,Q^{1m'n'}+P^{2\mu'n'a}\,Q^{2m'n'}$$

In order to perform the integration for the three angular variables θ, ϕ *and* χ using incrementally measured data, the data point spacing for all three angles must satisfy the sampling criteria for each variables. Theoretical guidelines

978-88-907018-1-8/13/$31.00 ©2013 IEEE

are available to specify the angular spacing in θ and ϕ in terms of the radius of the minimum sphere (referred to as the MRE) that will completely enclose the antenna. Experimental tests on a given test antenna and probe can also be carried out to verify these guidelines by taking closely spaced data and comparing the far field pattern results when the data point spacing is increased. For an arbitrary probe and measurement radius, satisfying the sampling criteria for the χ variable would require measurements at small increments in χ and numerical integration of the data in χ. The required multiple measurements over the complete sphere for small increments in χ would be very time-consuming and the numerical integration could be both time-consuming and inaccurate. To solve this problem, Wacker(4) proposed using a special probe that would have a symmetry in its far field pattern such that the spherical mode coefficients for the probe would be zero for all μ values except $\mu = \pm 1$. Such probes are referred to as first-order probes. When the probe satisfies this condition, measurements are only required for $\chi = 0$ and 90 deg and numerical integration of the data for the χ variable is not required. This greatly reduces the measurement time and results in a fast, efficient and accurate numerical technique to perform the calculations defined in equation 2. The vast majority of the software used in processing spherical near-field data uses this numerical technique and the assumption that the probe satisfies the $\mu = \pm 1$ requirement is implicit in using this software. Probes can be constructed which satisfy this requirement to a very high degree by using a circularly symmetric probe aperture and a precise transition from rectangular to circular waveguide. The spherical mode coefficients for $\mu \neq \pm 1$ of carefully constructed probes are typically at least 40 dB below the first order modes. But such special probes increase the cost of the measurement system and the probes may have a smaller bandwidth than similar rectangular open ended waveguide probes (OEWG). It has been established that if the measurement radius is large enough, probes such as the OEWG can be used for spherical near-field measurements, the effect of their higher order modes will be negligible and the efficient data processing algorithms can be used without causing a significant error in the results. There is only limited information on how large the radius must be and what the residual effects of the higher-order modes are (5) – (9). This study was undertaken to try and answer some of those questions using a technique that had not been tried before and that should be a very sensitive test of the probe's μ-mode properties.

II. SIMULATION CONCEPT

Ideally it would be desirable to perform a series of spherical near-field measurements using two separate probes having identical far field patterns except for their pattern characteristics for rotation about the z-axes of the probes. One probe would satisfy the first order mode requirements and have non-zero spherical mode coefficients for only $\mu = \pm 1$. The second probe would have the same on-axis axial ratio and tilt angle and the same spherical mode coefficients for the $\mu = \pm 1$ modes. However it would also have non-zero spherical mode coefficients for other μ values. This type of probe is referred to as a higher-order probe. Complete spherical near-field measurements could be performed for different test antennas and measurement radii using the two different probes and the far field patterns calculated using the same efficient numerical algorithms which use only the $\mu = \pm 1$ probe coefficients. A comparison of the patterns, polarization, gain and other parameters could then be used to quantify the effect of the higher-order probe when using the software that assumes the probe is a first-order probe.

Another conceptual measurement comparison would require fewer measurements and perhaps be a more sensitive test for the effect of differences in the two probes since it focuses on the specific near-field data that should be most sensitive to the probe characteristics described by the μ coefficients. In this measurement, the first-order probe would be placed at a fixed radius and a fixed θ *and* ϕ position on the measurement sphere. The probe would then be rotated about its z-axis in small increments and the received amplitude and phase recorded as a function of the rotation angle χ. This would produce a near-field polarization curve similar to those shown in Figure 4. The same measurement would be repeated with the higher-order probe and the polarization patterns could then be compared and the differences used to estimate the effect that the higher-order probe would have on far-field results. This measurement comparison could then be repeated for other radii and θ *and* ϕ positions and for other test antennas. This measurement should be very sensitive to the μ mode properties of the probe since it is the probe's property due to rotation about its z-axis that is different, the measurement involves only a rotation of the probe about its z-axis, and the measured data will have a large dynamic range in both amplitude and phase. While both of these measurements will be affected by measurement errors such as scattering, positioning errors, leakage and random errors, that may in fact be larger than the probe mode affects being tested, the latter technique may be less sensitive to these measurement errors since it is performed at a single position and requires much less measurement time.

An actual measurement of either type is not practical however since it is not possible to construct two different probes that are identical in every respect except their μ-mode coefficients. And since the effect that is being investigated is likely very small for some measurement configurations, any small imperfections in the construction of the probes would lead to erroneous results.

It is possible to simulate the second measurement to a very high precision that will not be affected by measurement errors or imperfections in the construction of the probes. The simulation can also be accomplished using actual test antennas and probe data and accommodate computations for large data arrays within a reasonable amount of time. The steps in the simulation are as follows.

A near-field data file is selected for the antenna under test that contains both main and cross-polarized data from a previous measurement. The data is processed using the standard near-to-far field transformation that includes a correction for the effect of the measuring probe. The far electric field pattern is computed producing the Ludwig II AZ and EL (10) vector components on a grid that is equally spaced in $\frac{k_x}{k}$ and $\frac{k_y}{k}$ over the span from -1 to +1 for a planar data file or over the full sphere using AZ and EL angles for a spherical data file. The resulting data is saved in an output file for further processing. Since the simulation polarization pattern results will not be compared to any actual measured data, this far-field data file is an error-free representation of a hypothetical antenna that is similar to the antenna used in the actual measurement. Measurement errors due to multiple reflections, truncation, scattering, position errors, flexing cables and probe correction are present in the measured data and the far field patterns. But the far-field pattern produced represents a hypothetical antenna, and since the same data will be used for both simulated probes, the measurement errors will have no effect on the comparison that will be calculated other than being for a specific hypothetical antenna. Other data sets can also be used to represent different test antennas.

A previously measured spherical near-field data file is then selected where a rectangular OEWG was the antenna under test and measurements had been performed at the same frequency as the above measurements. This measured data is processed using the spherical transformation software to produce a far-field pattern where the Ludwig II θ and ϕ vector components are calculated and saved using a spherical coordinate grid in θ and ϕ where θ varies from 0 to 90° and ϕ varies from 0 to 360°. Angular increments from 0.1° to 1° were used so that different pattern resolutions could be tried in the simulation. One set of output files filtered the spherical mode coefficients in the θ -index n using the MARS (11) – (12) processing to reduce the effect of scattering and produce smoother patterns as a function of θ , but no filtering was applied to the spherical mode coefficients as a function of the m-index which corresponds to the μ -index when the OEWG is used as a probe in a spherical measurement. These output files then represent an error-free far-field pattern for a hypothetical OEWG probe that includes all of the modes for a higher order probe.

A second set of probe output files were also produced using the same angular spans and spacing and the same MARS processing and filtering in the θ -index n as the first set. But for these output files, filtering was also applied to retain only the m = ±1 spherical modes in the calculation of the far-field pattern. These files then represent an error-free far field pattern for a hypothetical probe that is identical to the first probe except for the elimination of the higher-order μ mode coefficients. Figures 1 and 2 show the spherical mode amplitude plots for s=1 for the two probes.

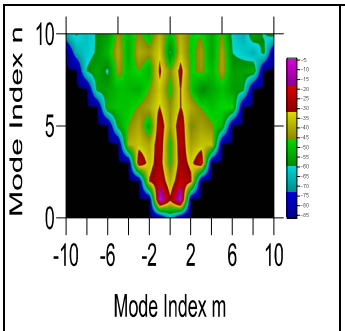

Figure 1-Spherical mode coefficient amplitudes for s=1 for higher-order probe with all m modes retained.

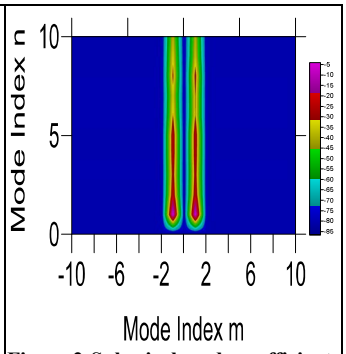

Figure 2-Spherical mode coefficient amplitudes for s=1 for first-order probe with only m = +1, -1 modes.

For the remaining steps in the simulation a computer program was developed to read in the data files for the antenna under test and the probes and produce a near-field polarization measurement at an arbitrary position for some measurement sphere. A polarization results was produced for both of the probes and then compared to determine the effect of the high order probe. The polarization curve was produced using the planar near-field transmission equation (13) which is shown in equation 3.

$$b_0'(x,y,z,\chi) = F' a_0 \iint \vec{t}_{10}(\vec{K}) \bullet \vec{s}_{02}'(\vec{K},\chi) e^{i\gamma z} e^{i(k_x x + k_y y)} dk_x dk_y$$

where

a_0 = Input amplitude and phase to AUT

$b_0'(x,y,z,\chi)$ = Probe output amplitude and phase for probe at (x,y,z) and rotated about the probe z-axis by the angle χ

$\vec{t}_{10}(\vec{K})$ = AUT plane-wave transmitting spectrum

$\vec{s}_{02}'(\vec{K},\chi)$ = Probe plane-wave receiving spectrum for χ rotation

(3)

The rotation angle χ has been added as a variable to the probe output and the probe receiving spectrum to show that the transmission equation will be used to produce polarization data by evaluating the equation using a series of rotated probe patterns. The planar transmission equation can be used for the simulation as well as the spherical transmission equation since both are equally valid and accurate expressions for the transmission between a test antenna and a probe at any arbitrary near-field position and relative orientation. The planar equation is much easier to calculate numerically and can be used without modification for both first-order and higher-order probes.

In the previous study, planar near-field data was used to produce a single plane-wave spectrum file for the AUT on a k-space grid with the main beam along the Z-axis. The different simulation cases were produced by using different x, y, and z-coordinates in equation (3). Each case represented one point of a spherical near-field measurement grid with the probe at a different field level relative to the peak. Conceptually, the probe was at the on-axis, $\theta = \varphi = 0$ position and the AUT was translated relative to the spherical origin by the x and y values

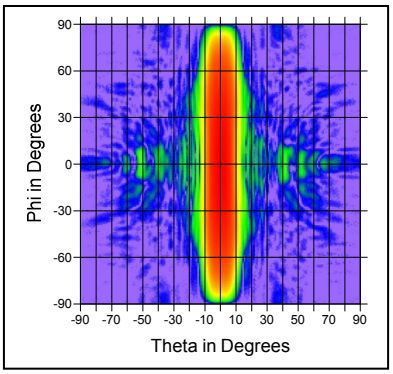

Figure 3 Central region of near-field amplitude for slotted array AUT.

used in the simulation. This made the simulation process more efficient since the same AUT file was used for all cases, but each case was then for a different location of the AUT in the measurement sphere. The results in the current simulations use spherical near-field data to produce the AUT plane wave spectrum file so that the simulations are for both on-axis and off-axis probe θ-positions but for the same location of the AUT in the measurement sphere. This is accomplished by using spherical rather than planar near-field data to produce the AUT far-field pattern over a complete sphere using the Ludwig II AZ/EL vector components and coordinates. The pattern includes the amplitude and phase for both main and cross components over the complete sphere. The resulting file is saved and read into the simulation program that rotates the pattern in Azimuth by a specified amount, calculates the plane wave spectrum from the far-electric field and interpolates to a k-space grid with specified dimensions. This spectrum is then used in equation (3) for $\vec{t}_{10}(\vec{K})$ to calculate the probe output as a function of the probe rotation angle and produce the near-field polarization curves.

The steps in the computer program will be described and illustrated for a specific example. The spherical near-field amplitude plot for the AUT is examined to select the azimuth offset angle that will be used in the simulation. Figure 3 shows a plot for the 24λ slotted waveguide array operating at 9.375 GHz that was used for the first simulations. Offset angles of 0, 10, 20 and 30 degrees were used for the simulations since these were for a range of amplitudes that would be representative of data that have the major effect on the far-field pattern. The probe pattern data file for the higher-order probe using spacing in θ of 0.2° and a ϕ spacing of 0.1° is read into the program. The probe pattern is rotated about the z-axis in small increments that are multiples of the ϕ spacing by translating the elements of the data array for each iteration of the program. For the first iteration the rotation is zero. This probe rotation, and the evaluation of the transmission equation for each rotated probe pattern, produces the polarization pattern by producing a probe output for each rotation increment. Interpolation is used on each of the probe patterns to calculate θ and ϕ vector components on a grid that is equally spaced in $\frac{k_x}{k}$ and $\frac{k_y}{k}$ with Nx x Ny points over the span from -1 to +1 and is identical to the grid that was used for the AUT plane wave spectrum. The AZ and EL vector components are then calculated from the θ and ϕ vector components. Since the receiving plane wave spectrum $\vec{s}'_{02}(\vec{K},\chi)$ is identical to the far electric field pattern, the probe patterns for each rotation angle required for the transmission equation have now been produced. The dot product of the AUT transmitting and probe receiving spectra, which is referred to as the coupling product, for each rotation angle is calculated at each point in the grid, the exponential factors involving the specified x, y, and z position and the components of the propagation vector are also calculated for each point and multiplied by the spectral product as required in equation (3) to produce the convolution product. The convolution product is then summed over all Nx x Ny points of the k-space grid to produce the probe received signal for the specified AUT rotation and z-distance as a function of the rotation angle χ and this polarization data is saved for comparison to the polarization data that will be produced using the first-order probe data.

When the polarization curve for the higher-order probe has been produced and saved, the probe pattern for the first-order probe which has only the spherical modes for m=±1 is read into the program and the polarization curve for this probe is produced. A sensitive and quantitative measure of the difference between the two probes is obtained by comparing the polarization curves produced by the two probes as illustrated in Figure 4. In the earlier study, only the amplitudes of the two curves were used to calculate a difference and this difference was then converted to an equivalent error/signal ratio. The error/signal ratio is a measure of the error that would occur in the spherical near-field data using the higher order probe and the numerical processing that assumes a first order probe. In the current study, the complex difference between the curves was calculated to include phase differences and the magnitude of the complex difference was then converted to the error/signal ratio shown in the following figures.

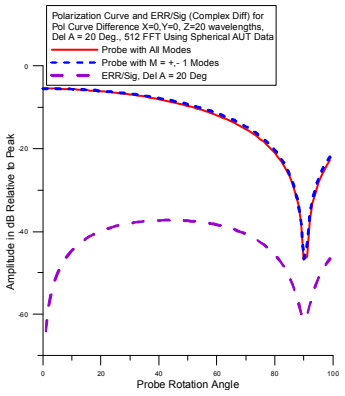

Figure 4 Polarization curves for two probes for AUT rotation of 20 degrees and z = 20 wavelengths.

When the simulation program was fully developed and producing output curves like figure 4, a number of tests were run to verify the accuracy of the concept and the programs. Two separate simulation programs were developed and tested. Both authors produced programs using different software but the same input data, the same concepts and equations. The results of the two programs were the same. Different resolutions were used for the initial probe patterns that were calculated using θ,φ coordinates. Angular increments as large as 1° for both angles were used with very little change in the output. All of the final results used 0.2° spacing in θ and 0.1° spacing in φ. The program was run for two z-distances corresponding to the radius of the minimum sphere and three times this distance to verify that the

difference between the two probes polarization curves decreased with distance showing that the higher-order probe performed like a first-order probe for larger separation distances. The results of these tests are summarized in Figures 5 and 6 which show the error/signal curves for four AUT azimuth rotation angles at the two z-distances. Similar results were obtained using a pyramidal standard gain horn as the AUT and these results will be shown when the paper is presented.

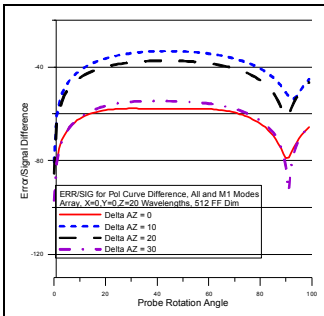

Figure 5 Error/Signal curves for z = 20 wavelengths and four AUT AZ rotation angles.

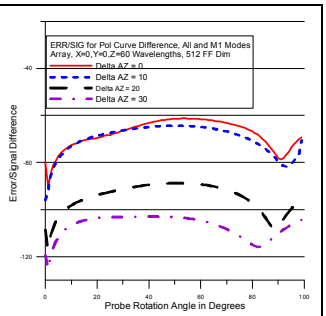

Figure 6 Error/Signal curves for z = 60 wavelengths and four AUT AZ rotation angles.

The on-axis amplitude and phase as a function of z-distance were also calculated for a single probe rotation angle to verify that these quantities varied as expected. In performing this tests, it was found that the array sizes for the AUT and probe that were used in calculating the planar transmission equation needed to be at least 1024 x 1024 to give correct results at Z distances of 80λ or larger. An example of the amplitude results for a standard gain as the AUT is shown in Figure 7. For large z-distances the oscillations in the curve are due to insufficient resolution in the plane wave spectra of the AUT and probe. For array dimensions less than 1024, the oscillations were larger and occurred at smaller distances.

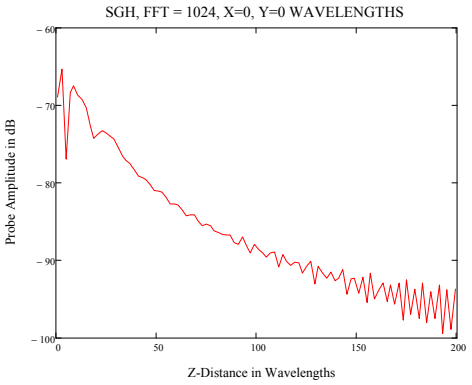

Figure 7 Probe amplitude versus z-distance for a standard gain horn and array dimensions of 1024.

Since the primary interest was for small z distances, this was not a limitation on the reliability of the results, and when larger z distances were used, the array sizes were increased as necessary.

The detailed shape of the difference curves like Figures 5 and 6 is not important. The overall level of the curve relative to the near field peak amplitude is a good measure of the probable error due to the higher order probe. And so to include the full range of the difference curve in the estimated error, the RMS value of the ERR/SIG difference between the polarization amplitude curves as measured by the first order and higher-order probes was calculated for each test antenna and probe position and this RMS value is used as a predictor of the probable error in the spherical near-field measurement at that particular point. From tables or graphs of the RMS value for a number of points in the near-field, conclusions can then be drawn about the overall measurement and calculation uncertainty. The results of these simulations for the two different antennas using a rotated AUT pattern that more closely simulates a spherical measurement and using the complex difference rather than just the amplitude gave results that are similar to the previous study. The conclusion is that the effect of using an OEWG probe in a typical spherical near-field measurement is probably below the error levels of other errors. This is true even when the measurement radius is close to the minimum sphere.

III References

(1) Newell, A.C., Gregson, S.F.," Estimating the effect of higher order modes in spherical near-field probe correction", AMTA 34th Annual Meeting & Symposium, Seattle, WA, Oct. 2012.
(2) Jensen, F. (1975), "On the probe compensation for near-field measurements on a sphere", *Archiv für Elektronik und Übertragung-stechnik*, Vol. 29, No. 7/8, pp. 305-308.
(3) Hansen, J.E. (Ed.) (1988), *Spherical Near-Field Antenna Measurements*, Peter Peregrinus, Ltd., on behalf of IEE, London.
(4) Wacker, P.F. (1974), "Near-field antenna measurements using a spherical scan: Efficient data reduction with probe correction", *Conf. on Precision Electromagnetic Measurements*, IEE Conf. Publ. No. 113, pp. 286-288, London, UK.
(5) T. A. Laitinen, S. Pivnenko, and O. Breinbjerg, "Odd-order probe correction technique for spherical near-field antenna measurements," *Radio Sci.*, vol. 40, no. 5, 2005.
(6) T. A. Laitinen and O. Breinbjerg, "A first/third-order probe correction technique for spherical near-field antenna measurements using threeprobe orientations," *IEEE Trans. Antennas Propag.*, vol. 56, pp. 1259–1268, May 2008.
(7) T. Laitinen, J. M. Nielsen, S. Pivnenko, and O. Breinbjerg, "On the application range of general high-order probe correction technique in spherical near-field antenna measurements," presented at the 2nd Eur. Conf. on Antennas and Propagation (EuCAP'07), Edinburgh, U.K., Nov. 2007.
(8) T. A. Laitinen, S. Pivnenko, and O. Breinbjerg," Theory and Practice of the FFT/Matrix Inversion Technique for Probe-Corrected Spherical Near-Field Antenna Measurements With High-Order Probes," *IEEE Trans. Antennas Propag.*, vol. 58,, No. 8, pp. 2623–2631, August 2010.
(9) T. A. Laitinen, S. Pivnenko,"On the truncation of the azimuthal mode spectrum of high-order probes in probe-corrected spherical near-field antenna measurements" AMTA, Denver, November 2012.
(10) A. C. Ludwig, "The definition of cross polarization," *IEEE Trans. AntennasPropag.*, vol. 21, pp. 116–119, Jan. 1973.
(11) Hindman, G, Newell, A.C., " Reflection Suppression in a large spherical near-field range", AMTA 27th Annual Meeting & Symposium, Newport, RI, Oct. 2005.
(12) Hindman, G, Newell, A.C., " Reflection Suppression To Improve Anechoic Chamber Performance", AMTA Europe 2006, Munch, Germany, Mar. 2006.
(13) Kerns, D.M. (1976), "Plane-wave scattering.matrix theory of antennas and antenna-antenna interactions : formulation and applica-tions", *J. Res. NBS*, Vol. 80B, No. 1, pp. 5-51.